Macromolecular Symposia
www.ms-journal.de

Study of Anticancer Properties of Graphene Oxide–Metal Oxide Composite

*Shweta D. Dabhi, Swati Gahlot, Sheefa Mirza, Medha Pandya, Rakesh Rawal, Vaibhav Kulshrestha, and Prafulla K. Jha**

Graphene and graphene oxide (GO) have garnered significant attention due to their exceptional properties. GO, enriched with various functional groups such as epoxy, hydroxyl, and carboxylic groups, has exhibited remarkable potential in biomedical applications. The combination of GO with metals has proven to be a promising platform for cellular imaging, with this study focusing on the preparation of diverse hybrids of GO with metal oxides (GO/MO) and their potential as anticancer agents. In this research, GO is functionalized with MOs like TiO_2, Fe_3O_4, and Cu_2O using specific chemical methods and investigated for the anticancer activity for the application as cancer therapeutic agent. The resulting GO/MO hybrids exhibits favorable thermal and mechanical properties. Moreover, their cytotoxicity against human lung cancer cells is assessed in vitro, revealing the promising anticancer activity of GO/MO hybrids. Notably, the GO/Cu_2O hybrid demonstrates particularly high cytotoxicity in human lung cancer cells.

1. Introduction

Graphene and graphene oxide (GO) has been capturing a great deal of attention in variety of research fields such as physics, chemistry, material science as well as life science.[1] Unveiling its remarkable properties like mechanical, thermal, optoelectronic, chemical as well as large surface area, graphene can be used in wide range of applications including energy conversion and storage devices.[2–4] The promising and versatile method to produce graphene or reduced graphene oxide (rGO) is by chemical exfoliation of graphite and reduction of GO, which is one of the major advantages of GO for mass production of graphene.[5–7] Over the past few years, research on drug delivery has attracted a great attention of many researchers. GO provides a new platform with admirable opportunities for the development of carriers for drug and gene delivery,[8–10] cell imaging, and photo-therapy of cancer.[11–13] To improve the properties of material and to use GO for a specific application, composites with metal or metal oxide (MO) can be prepared. The nanocomposites help in understanding of fundamental properties of hybrid nanostructures for their potential applications.

Lung cancer represents a major global health concern, and the use of human lung cancer cell lines aligns the research with the disease's actual clinical context. Understanding the

S. D. Dabhi
Department of Physical Sciences
P. D. Patel Institute of Applied Sciences
Charotar University of Science and Technology
Changa, Gujarat 388421, India

S. D. Dabhi, S. Gahlot
Department of Physics
Maharaja Krishnakumarsinhji Bhavnagar University
Bhavnagar, Gujarat, India

S. Gahlot
Department of Physics
Sardar Vallabhbhai National Institute of Technology
Ichchhanath, Surat, Gujarat 395007, India

S. Mirza
Department of Internal Medicine
Faculty of Health Sciences
University of Witwatersrand
Johannesburg, South Africa

S. Mirza, R. Rawal
Department of Lifesciences
Gujarat University
Ahmedabad, Gujarat, India

S. Mirza, R. Rawal
Department of Cancer Biology
The Gujarat Cancer and Research Institute
Ahmedabad, Gujarat, India

M. Pandya
Department of Lifesciences
Maharaja Krishnakumarsinhji Bhavnagar University
Bhavnagar, Gujarat, India

R. Rawal
Department of Biochemistry and Forensic Science
Gujarat, India

V. Kulshrestha
CSIR-Central Salt and Marine Chemicals Research Institute
Bhavnagar, Gujarat 364002, India

P. K. Jha
Department of Physics
Faculty of Science
The MS University of Baroda
Vadodara, India
E-mail: prafullaj@yahoo.com

The ORCID identification number(s) for the author(s) of this article can be found under https://doi.org/10.1002/masy.202300086

DOI: 10.1002/masy.202300086

complex genetic and environmental factors driving its pathogenesis is paramount for effective prevention and treatment strategies. Nanomaterials have emerged as promising tools in the fight against lung cancer, offering innovative approaches to diagnosis, treatment, and monitoring. Numerous nanomaterials have been employed as cutting-edge carriers for cancer treatment. Carbon based nanomaterials, e.g., graphene, carbon nanotubes have been used a lot in biological applications.[14] One of the active research fields in nanotoxicology is the interaction between nanoparticles and living things and the biological reactions that follow.[15] In a study by Montes-Duarte et al., GO, as well as silver, ceria nanoparticles, and combinations of these materials, have been thoroughly examined and assessed for their effectiveness in deactivating *Escherichia coli* and *Salmonella* Typhimurium.[16] The integration of silver and ceria nanoparticles with GO significantly enhanced its performance, resulting in elevated inactivation rates and reduced exposure times required to achieve complete deactivation. Cuprous oxide (Cu_2O) is a well-known p-type semiconductor with a narrow band gap of 2.0–2.2 eV, high optical absorption. It exhibits fast recombination of the photo-generated electron–hole pairs and therefore can be used in photocatalysis, high performance electrode, solar cell, hydrogen production,[17–19] organic contamination degradation under visible light,[20,21] etc. Further, Cu_2O is less toxic, abundant, inexpensive, and easily manufactured which makes it prime candidate for the decomposition of water and degradation of organic pollutants. Synthesis of CuO nanoparticles and CuO-GO nanocomposites using an environmentally friendly approach using abundant and eco-friendly *Acalypha indica* plant has been done for investigating.[22] This study demonstrated the potential of prepared nanocomposites as catalysts in photocatalytic and anti-cancer activities. Notably, the cytotoxic activity showed a remarkable 70% inhibition rate against HCT-116 human colon cancer cells at a concentration of 100 μg mL^{-1}. Development of a bimetallic mixed MO employing nitrogen-doped graphene oxide (N-GO) and nickel oxide and copper oxide (NiO/CuO) led to the production of NiO/CuO/N-GO nanocomposite.[23] Additionally, the nanocomposite's potential for antibacterial and anticancer properties was looked into. *E. coli*, *Staphylococcus aureus*, and *Bacillus cereus* were each inhibited by NiO/CuO/N-GO (50 g mL^{-1}) with inhibition zones of 18.5, 15.25, and 17.5 mm, respectively. NiO/CuO/N-GO nanocomposite's anticancer ability and impact on cell cytotoxicity were assessed in both normal HEK293 human embryonic cells and A549 human lung cancer cells. Dual labeling with ethidium bromide and acridine orange was used to determine cell viability. The NiO/CuO/N-GO composite's anticancer potential was confirmed by a study on the formation of reactive oxygen species.

Composites of GO with titanium dioxide (GO/TiO_2), magnetite (GO/Fe_3O_4) have also received a great deal of attention for the application in anticancer therapy.[24,25] TiO_2, a well-known n-type semiconductor with a band gap of 3.0–3.2 eV, has been investigated as an excellent photocatalyst and mediated toxicity destroyer for the cancerous cells.[26,27] Further, it possesses a very less or no dark toxicity as revealed through in vitro and in vivo study.[28] GO/TiO_2/doxorubicin nanoparticles were effectively synthesized and evenly distributed within the carbon layers of GO sheets.[29] The findings revealed that an increase in the ratio of PLA to chitosan, TiO_2 content, and GO/TiO_2/DOX content led to a slower release rate of DOX over time. The release of DOX from nanofibers with a thickness of 10 μm followed non-Fickian diffusion, while nanofibers with thicknesses of 30 and 50 μm followed Fickian diffusion. Furthermore, the results from cell viability assays indicated that the inhibitory effect on the proliferation of target cancer cells was intensified with higher DOX content in the chitosan/PLA/TiO_2/DOX/GO nanofibers. The chitosan/PLA/TiO_2/DOX/GO nanofibers, when combined with an external magnetic field, demonstrated enhanced killing of A549 cancer cells.

However, from the all known materials which show anticancer activity, magnetic nanoparticles are introduced as an excellent candidate for the biological imaging or separation.[30,31] Magnetic nanoparticles have been utilized for drug and gene targeting,[32] separation of proteins, DNA and cells from samples,[33,34] as magnetic biosensors,[35] in cancer therapy as heat mediator.[36] Fe_3O_4 possesses large surface area with reactive surface, it is easily separable by magnetic field, both magnetically and chemically stable and owes very less toxicity.[37,38] Furthermore, Fe_3O_4 can be self-assembled in the presence of external magnetic field which indicates that it can be controlled as required when external field is applied.[39] In a study, a simple method was employed to create a superparamagnetic graphene oxide (SPMGO) nanocomposite using a chemical precipitation technique. The nanocomposite was easily modified by incorporating cyanuric chloride as a connecting agent for drug loading.[40] The in vitro compatibility with blood of the covalently immobilized methotrexate (MTX) on the modified nanocarrier was contrasted with the physical immobilization of MTX on the unmodified nanocarrier. The cytotoxicity test demonstrated that SPMGO/CC/MTX exhibited the most significant anti-tumor activity against Caov-4 cells, reaching an impressive 89%. Moreover, based on the overall results, the combination of high drug loading, potent toxicity against tumor cells, optimal drug release, and blood compatibility contributed to enhanced therapeutic effectiveness. Regarding its properties, the synthesized nanocarrier can serve as an innovative option for controlled drug delivery, facilitating targeted drug release, MRI imaging, and magnetic field-guided targeted therapy.

In line with the interactive research on GO with oxide nanocomposites, we have reported an approach for the facile preparations of GO decorated with TiO_2, Fe_3O_4, and Cu_2O separately. GO/MO nanocomposites were synthesized using chemical methods. Various characterization techniques have been applied to study the structure and morphology of prepared GO/MO hybrid nanocomposites. Due to interaction between GO sheets and nanoparticles, it enables fast electron transport from particle to carrier inducing enhanced electrochemical performance. Anticancer activity of GO and GO/MO hybrids are investigated in order to study the role of MO hybrid for their possible application as cancer therapeutic agent. To assess the cytotoxic potential of GO and its composites, lung cancer cell line (A549) was used for the present study.

2. Result and Discussion

2.1. Structural Analysis

XRD, SEM, and TEM are the essential tools to determine the structure, crystallinity, particle size, and morphology of the

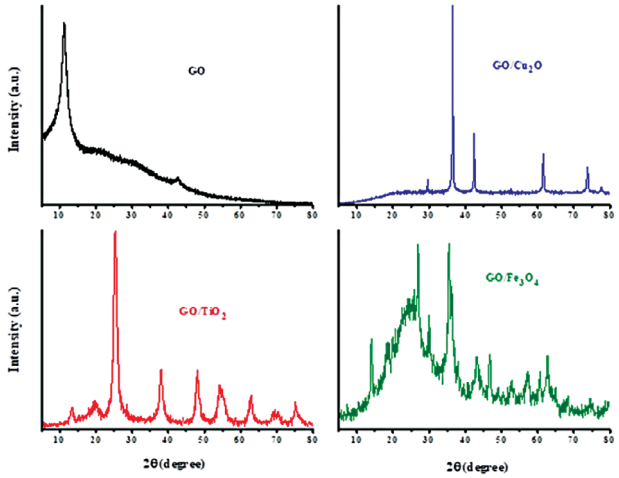

Figure 1. XRD patterns of graphene oxide (GO), GO/TiO_2, GO/Fe_3O_4, and GO/Cu_2O.

nanostructures. XRD patterns of GO, GO/TiO_2, GO/Fe_3O_4, and GO/Cu_2O nanocomposites are depicted in **Figure 1**. In XRD pattern of GO prepared via modified Hummer's method, a characteristic peak at 11.2° is visible. It corresponds to (001) crystal plane of GO with d-spacing of 7.9 Å. Compared to graphite, peak of GO shifts to lower degree due to oxidation. For GO and its composites, broad peaks of XRD suggests nanocrystalline size of GO/MO composites. In GO/TiO_2, XRD peaks at 20° is due to rGO and peaks at 25.29°, 48.03°, 54.27°, 62.92°, and 71° are attributed to the diffractions of facets (101), (200), (105), (204), and (220) of TiO_2. GO/Fe_3O_4 shows peaks at 14.2° and 26.6° correspond to GO and rGO, respectively. XRD diffraction peak at 30.1°, 35.4°, 43.2°, and 62.8° corresponds to (220), (311), (400), and (440) planes of cubic Fe_3O_4.[41] For GO/Cu_2O peaks obtained at 29.57°, 36.46°, 42.36°, 61.52°, 73.71°, and 77.5° correspond to diffraction planes at (110), (111), (200), (220), (311), and (222) of Cu_2O as per JCPDS No.78-2076 similar to the results obtained by ref. [41].

Using SEM and TEM analysis, the morphology and structure of pristine GO and its nanocomposites with MO were characterized. **Figures 2** and **3** show SEM and TEM images respectively for GO and GO/MO hybrids. Firstly, considering the pure GO particles TEM shows the formation of two-dimensional smooth sheets. Similarly, from SEM (Figure 2a) we can observe similar flakes like structure randomly aggregated with distinct edges, wrinkled surfaces, and folding. For the GO decorated TiO_2, low magnification TEM image as shown in Figure 3c clearly reflects uniformly distributed dark contrast dots which are due to the presence of nanosized TiO_2 over GO surface. The outline of GO and embedded nanoparticles can be easily differentiated. The crystallographic structure of GO/TiO_2 can be confirmed using selected area electron diffraction (SAED). The SAED pattern taken from nanocomposites showed polycrystalline nature. There is uniform distribution of TiO_2 nanoparticles in GO plane. In SEM image of GO/TiO_2 shown in Figure 2b, GO had a sheet-like structure with thick sheets, smooth surfaces, and wrinkled edges. It is clearly observed that TiO_2 spheres were supported on the surface of GO sheets.

In GO/Fe_3O_4, compared to the pristine GO, it is distinctly seen that Fe_3O_4 nanoparticles were embedded into GO surfaces to make nanocomposite structure without any obvious aggregation in Figure 3e,f. Most of the Fe_3O_4 nanoparticles are highly dispersed on GO sheet. The SAED pattern indicates that magnetite nanoparticles are polycrystalline in nature. It is worthwhile that there are no large areas of GO sheet without Fe_3O_4 nanoparticles decorated on the surface and no traces of aggregation onto the surface could be observed.

Cu_2O nanoparticles have spherical morphology as clearly seen from SEM image (Figure 2c). Compared to GO, the strengthening effect of GO/MO is appreciable when processed by molecular-level mixing with metal. Likewise other embedded composites of GO, GO/Cu_2O composites characterized by SEM shows the implantation of GO within the matrix where smooth surface of GO is covered with small Cu_2O particles. It is further confirmed via TEM, there is Cu_2O particles surrounded throughout the matrix with little agglomeration. High resolution TEM image in Figure 3g,h shows GO sheets with decoration of Cu_2O.

2.2. Spectroscopic Characterization

In the spectroscopic analysis of any material, electromagnetic radiation interacts with matter which reveals the useful information related to vibrations of material. FTIR and Raman spectroscopic investigation were carried out for prepared GO and GO/MO nanocomposites. Raman spectroscopy is a fingerprint characterization to identify vibrational, rotational, and other low frequency modes in material.

Figure 4 shows the obtained results for Raman spectra of GO, GO/TiO_2, GO/Fe_3O_4, and GO/Cu_2O. Raman spectra of GO clearly shows well referred D band and G band at 1353 and 1600 cm^{-1}, respectively. D band is due to the distorted structure in graphene in presence of sp^3 defects. Thus, it measures the disorder in sp^2 hybridized carbon sheet. The G band at 1600 cm^{-1} represents E_{2g} mode which arises due to the in-plane stretching of C–C bonds and commonly observed in sp^2 carbon systems. Decrease of Raman shift in D band and G band for GO/MO composites is clearly observed. In GO/TiO_2 sample, Raman peaks at 145 and 631 cm^{-1} due to E_g mode, at 396 cm^{-1} represents B_{1g} mode and B_{1g} + A_{1g} mode at 514 cm^{-1}confirms the presence of anatase phase of TiO_2. For GO/Fe_3O_4, spinel ferrite structure of Fe_3O_4 give rise to three T_{2g}, one E_g, and one A_{1g} mode. Raman peak corresponding to 485 cm^{-1} is due to doubly degenerate T_{2g} mode. For Cu_2O/GO, peaks at 146, 520, and 630 cm^{-1} which can be well described for T_{1u}, T_{2g}, and T_{1u} mode, respectively.[42]

FTIR is a vibrational spectroscopic technique used to obtain an infrared spectrum of absorption or emission of any material. **Figure 5** shows FTIR spectra of GO, GO/Fe_3O_4, and GO/TiO_2 hybrids. As discussed earlier, GO possesses various oxidizing functional groups (Figure 5a). Therefore, several peaks corresponding to different functional groups are observed. Due to unoxidized graphitic plane, C = C vibrations at 1622 cm^{-1} is observed. Peaks at 1064 and 1227 cm^{-1} correspond to alkoxy and epoxy (C–O) stretching vibrations. While peaks at 1397 and 1720 cm^{-1} are due to the carboxylic and ketonic (C = O) groups, respectively. Due to the extensive oxidation, a strong and broad O–H stretching vibration peak at 3396 cm^{-1} in GO is clearly visible.

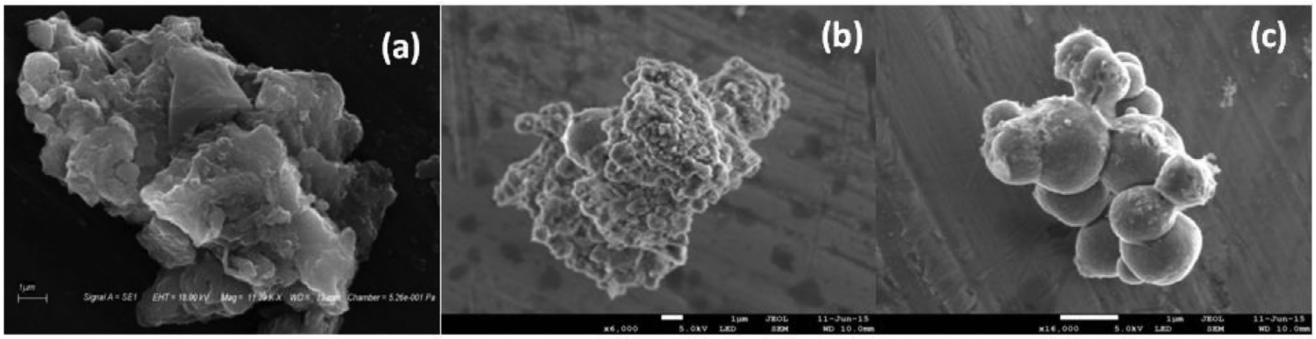

Figure 2. SEM micrographs of a) graphene oxide (GO), b) GO/TiO_2, and c) GO/Cu_2O.

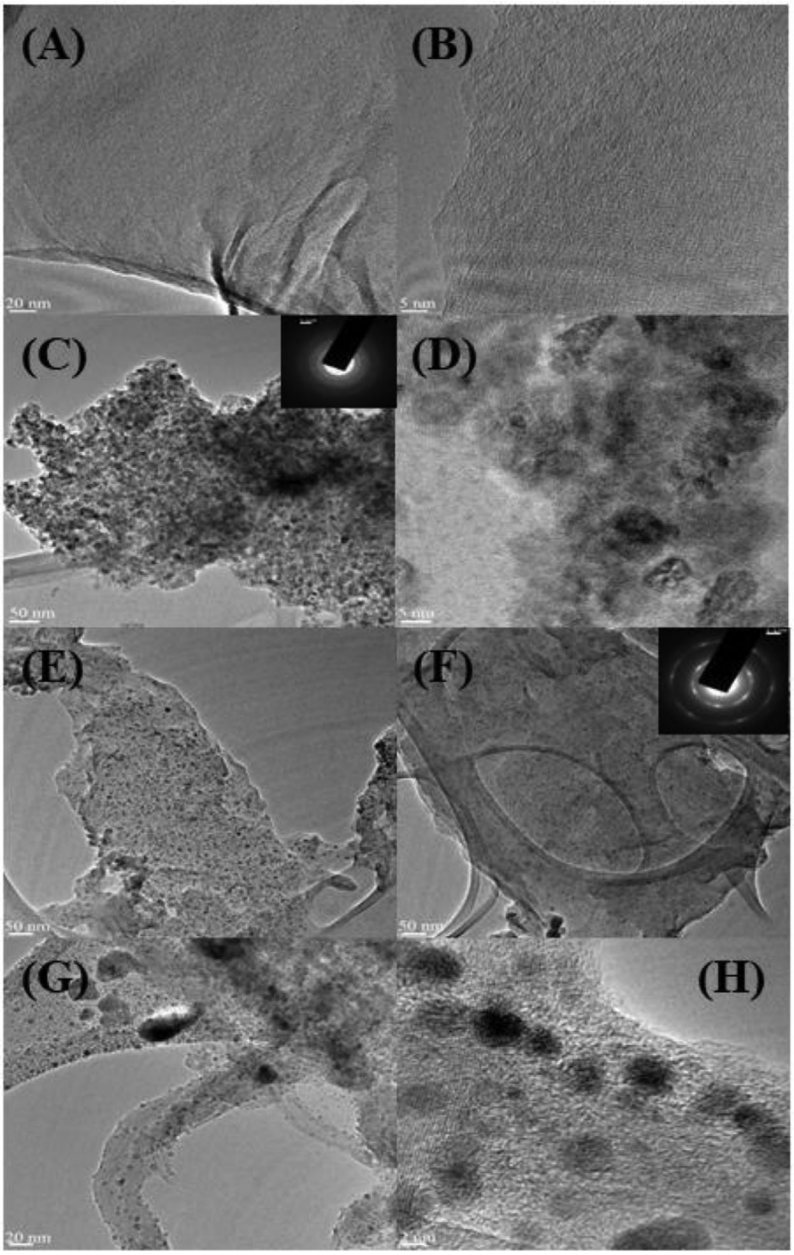

Figure 3. TEM images of A, B) graphene oxide (GO), C, D) GO/TiO_2, E, F) GO/Fe_3O_4, and G, H) GO/Cu_2O.

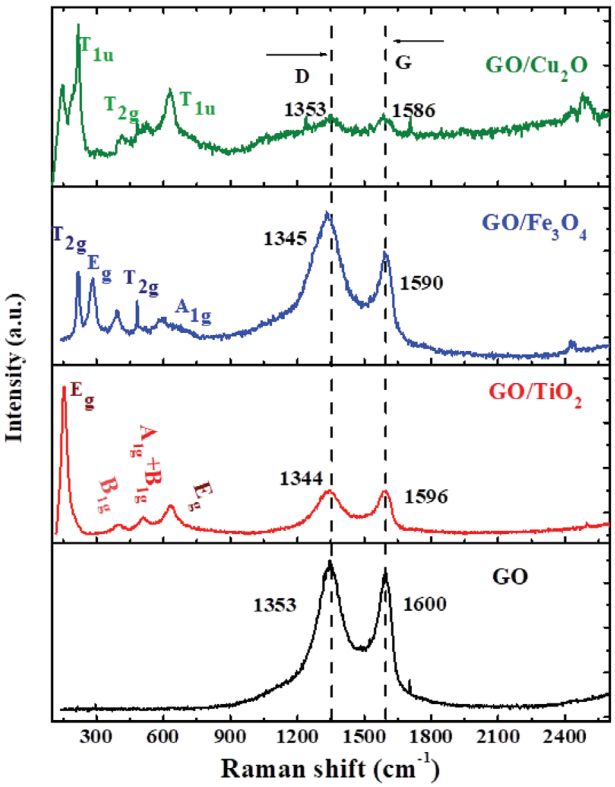

Figure 4. Raman spectra of graphene oxide (GO), GO/TiO_2, GO/Fe_3O_4, and GO/Cu_2O.

For GO/MO hybrid nanocomposites, vibrational modes as discussed for GO FTIR spectra are also observed with slight variation in wavenumber. For GO/Fe_3O_4, a new peak at 467 cm^{-1} arises due to stretching vibration of Fe–O bond while for GO/TiO_2 composite, Ti–O vibrational mode is observed for 658 cm^{-1} (Figure 5b, c).

2.3. Thermal Stability

The thermal stability of synthesized GO and GO/MO hybrid composites were evaluated by TGA. This analysis is helpful to trace behavior of material at higher temperature to determine the thermal stability, oxidation/reduction, and combustion, etc.

Figure 6 displays TGA curves of GO and GO/MO hybrids. As observed in earlier experiment for GO,[43] approximately 35% weight loss occurs at 200°C which is due to the decomposition of oxygen containing functional groups present in GO. The loss at higher temperature can be attributed to the removal of more oxygen containing groups present in GO. Weight loss of GO/TiO_2 is only 15% up to 400°C. The results are comparable to reported literature for rGO-anatase TiO_2 by Wang et al.[44] 10% thermal reduction in mass of GO/Fe_3O_4 could be attributed to the loss of the adsorbed H_2O. GO/Cu_2O being thermally quite stable and only 10% weight loss is observed upto 600°C due to higher stability of CNT. Overall, an increase in thermal stability is clearly depicted from figure for GO/MO nanocomposite compared to GO.

2.4. Anticancer Activity of GO/MO Hybrids

The discovery of nanomaterial graphene in 2004 has fascinated much responsiveness for potential biomedical applications like gene therapy and drug delivery.[45] The in vitro anticancer activity of GO and three GO/MO nanocomposites were evaluated using MTT assay with A549 cells. Cancerous cells were introduced to GO and GO/MO hybrid for 24 h for different concentration of doses and so obtained are described **Figure 7**. The viability of the untreated lung cancer cells (without compounds) was set as 100%, and the viability of the compound-treated A549 cells was calculated in accordance.

As shown in Figure 7, the compounds GO, GO/TiO_2, and GO/Fe_3O_4 have negligible cytotoxicity to cells at lower concentrations. Even when the concentration is six to eight times higher, the cytotoxicity of the GO/MO hybrids is still very low except GO/Cu_2O. GO unveiled slight viability cost toward A549 cells. Even though at the significant concentration (400 μg mL^{-1}), the viability of cells remained above 45% after 24-h exposure (Figure 7a), it was found that the IC_{50} of GO was 230 μg mL^{-1} against malignant cells and suggested that the concentration of GO did not significantly diminish the viability of cells after 24 h. The low cytotoxicity of GO was possibly accredited to the fine oxygen atoms in the form of carboxyl, epoxy, and hydroxyl groups on the surface of GO.[46] To date, several approaches resembling that different parameter like size, the shape of the GO flacks are the factors affecting the cell viability.[47]

In present study, GO/TiO_2 and GO/Fe_3O_4 nanocomposites did not cause significant decrease of cell viability and no 50% cell death is observed in 400 and 500 μg mL^{-1} range, respectively (Figure 7b, c). GO could enter A549 cells and located in the cytoplasm and nucleus without causing any cell damage. The TiO_2-GO composite separated into GO and TiO_2 after TiO_2-GO composite entered A549 cells.[48] The cytotoxicity of GO/TiO_2 composite was probably attributed to TiO_2 nanoparticles. In 2012, Zhen et al.[29] revealed that GO/TiO_2 composites have exceptional light driven photodynamic anticancer activity without dark cytotoxicity. As reported by Wang et al.,[49] the Fe_3O_4/GO has good drug loading capacity however do not show toxicity even at higher concentration. Chemically and thermally reduced GO demonstrated significant in vitro anticancer activity.[50] In this study, GO/Cu_2O nanocomposite has more prominent inhibitory effect on the cell viability with IC_{50} of 11.22 μg mL^{-1} (Figure 7d). The Cu_2O–reduced GO has great cytotoxic effect under visible and near-infrared light irradiation on lung cancer cells and normal cells which indicated photothermal effects.[22] However, obtained results depicted that GO/Cu_2O reveals good cytotoxic effects toward the malignant cell without any additional factor like irradiation of light, drug loading, and doping.

3. Conclusions

In summary, this study conducted an experimental investigation into GO and its composites with various MO (GO/MO). Using a chemical precipitation method, we successfully synthesized GO and three GO/MO nanocomposites – namely, GO/TiO_2, GO/Fe_3O_4, and GO/Cu_2O. These materials underwent extensive characterization, including XRD, SEM, TEM, FTIR, Raman, and TGA analyses, to probe their structural, spectroscopic, and

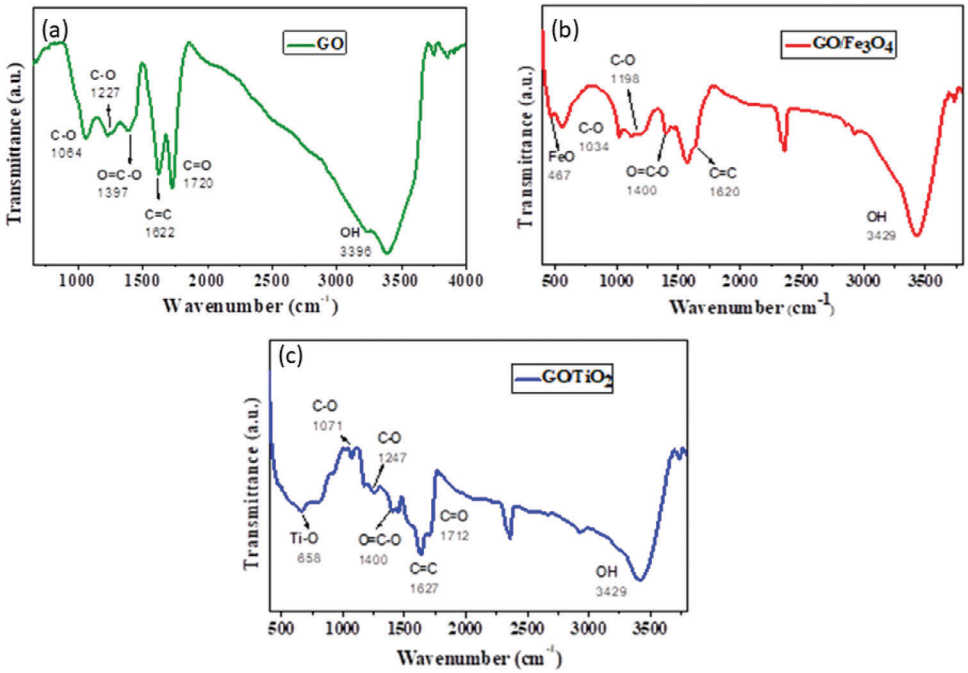

Figure 5. FTIR spectra of GO and GO/MO hybrid nanocomposites. GO, graphene oxide; MO, metal oxide.

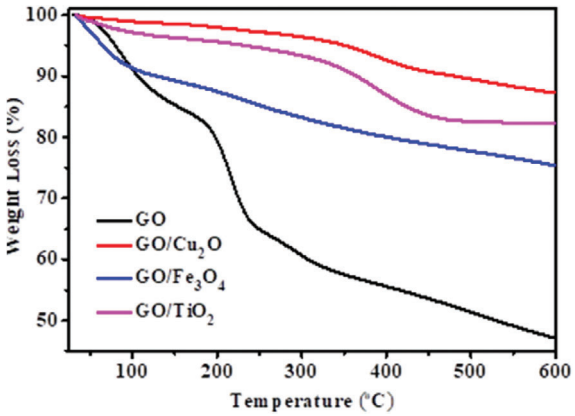

Figure 6. TGA curves of graphene oxide (GO), GO/TiO_2, GO/Fe_3O_4, and GO/Cu_2O.

thermal properties. The primary focus of this research was to explore the biomedical potential of graphene-based materials, particularly their anticancer activity. In vitro cytotoxicity assessments were performed on A549 cell lines across various nanocomposite concentrations using the MTT assay. Among all materials considered, GO/Cu_2O exhibited the highest cytotoxicity against human lung cancer cells, indicating its promising therapeutic potential for cancer treatment. These findings underscore the potential of GO–MO composites in advancing targeted and personalized cancer therapies. These innovative materials can synergistically enhance therapeutic efficacy, enabling multimodal imaging and treatment, and may also serve in gene delivery and immunomodulation strategies. As research progresses, addressing biosafety concerns, optimizing synthesis methods, and conducting thorough preclinical investigations will be pivotal steps toward translating these advancements into clinical applications. Such developments hold the potential to revolutionize cancer treatment by providing precise and effective interventions tailored to individual patient needs.

4. Experimental Section

Materials: Graphite powder was purchased from Acros Chemicals. Carbon nanotubes and poly acrylic acid were procured from TCI chemicals. Titanium isopropoxide (TTIP), $NaNO_3$, $KMnO_4$, $FeCl_3$, and $FeCl_2$ were obtained from SD Fine Chemicals India Ltd. All other reagents were of analytical grade and commercially purchased which were used without any further treatment.

Synthesis of Graphite Oxide: Graphite oxide was prepared by oxidizing natural graphite powder using Hummer's method.[51,52] A definite quantity of graphite and $NaNO_3$ powder were added to H_2SO_4 (98% conc.). This solution was kept in ice bath to maintain 0–5 °C temperature with continuous stirring for 2 h. Further $KMnO_4$ was gradually added to the solution and stirred for 2 h at room temperature. Distilled water was added to dilute the solution and stirred for another 2 h to increase the oxidation degree of GO. Finally, hydrogen peroxide solution (5% H_2O_2) and water were added and left overnight. The prepared graphite oxide was isolated by multiple washing with DI water in centrifuge to remove salt impurities, acid, etc. Synthesized graphite oxide was dispersed in distilled water and subsequently exfoliated using ultrasonication to obtain nano-GO.

Synthesis of GO/Fe_3O_4: Synthesis of GO/Fe_3O_4 was done as follow.[41] 0.7 g synthesized GO was dispersed in 450 mL of distilled water by ultrasonication for 1 h. 0.4 g $FeCl_3$ and 0.16 g $FeCl_2$ each dispersed in 25 mL distilled water were slowly added to above GO solution at room temperature. 30% ammonia was added dropwise to maintain the 10 pH of solution. Temperature was increased to 90 °C and 10 mL hydrazine was added followed by stirring for 4 h.

Synthesis of GO/TiO_2: GO/TiO_2 was prepared by the method described elsewhere.[44] 11.44 mL acetic acid, 0.44 g polyacrylic acid (PAA), and 88 mL (0.5 g L^{-1}) GO were mixed and stirred for 1 h at 60 °C. Titanium

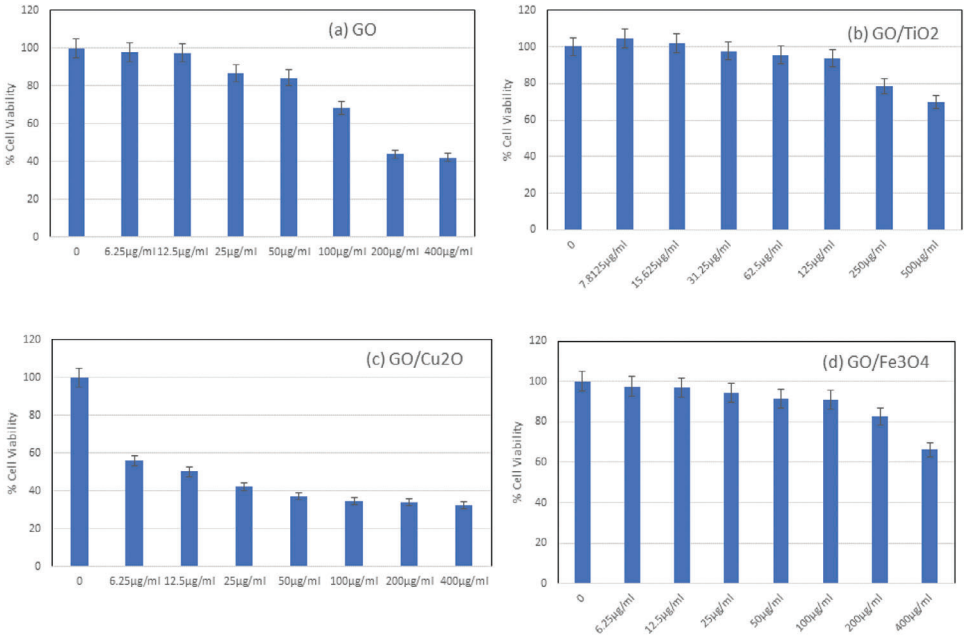

Figure 7. Cell viability for different concentration of GO and GO/MO hybrids. GO, graphene oxide; MO, metal oxide.

precursor (3.3 mL TTIP, 14.4 mL ethylene glycol, and 2.3 mL acetic acid) was added dropwise to the above solution. The whole solution was kept in microwave at 200 °C temperature for 45 min to get GO/TiO_2 nanocomposites. The obtained precipitate was centrifuged and washed with DI water to remove unwanted impurities and ions. The final precipitate was dried in oven at 50 °C.

Synthesis of GO/Cu_2O: Following method of Zeng et al.,[53] CNT was also assembled in GO/Cu_2O nanocomposites which showed the strong π–π interaction and resulted in stable suspension in water. Acid treated CNT was prepared by adding 0.1 g multi-walled CNTs in 255 mL aqua regia medium (sulfuric acid and nitric acid in 1:3 proportion) which was mixed with 30 mL GO solution (1 g L^{-1}). After keeping this solution in ultrasonic bath for 30 min, 25 mL gelatin was added and again sonicated for 30 min. 50 mL 0.7 M copper sulfate ($CuSO_4$) and 50 mL 0.5 M glucose were mixed and added to above solution. The whole solution was stirred for 15 min and then 30 mL 7 M sodium hydroxide ($NaOH_{aq}$) was added followed by heating for 10 min. As a result, reddish brown precipitate was collected which was centrifuged to separate precipitate and to remove unreacted reagents. The obtained precipitate was dried in vacuum at 80 °C to remove water content and get powder form GO/Cu_2O.

Cell Line and Culture Condition: Human lung cancer cell lines A549 were obtained from National Centre for Cell Science (NCCS), Pune. A549 cells were cultured in RPMI-1640 containing sodium bicarbonate, sodium pyruvate, and 25 mM HEPES buffer supplemented with 10% FBS (Cellclone), 1% v/v minimal essential medium nonessential amino acids (Hi-Media), and antibiotic & antimycotic (penicillin, streptomycin, and amphotericin B; Hi-Media) in humidified atmosphere of 5% CO_2 at 37 °C.

Cell Viability Assay: Cell counting kit-8 (CCK-8) was used to measure the cell proliferation and cytotoxicity. Cultured cell (A549 cell line) sample was centrifuged at 2500 rpm for 10 min and the supernatant was discarded. The resulting pellet was resuspended in appropriate amount of media and viability count was performed using trypan blue dye exclusion assay by automated cell counter TC10 (Bio Rad). Cells were plated in 96-wells at a final density of 1×10^4 cells per well. Cells were exposed to nanoparticles for 24 h. Cell counting kit-8 cytotoxicity assay (MTT) was performed to find out the effective concentration.

MTT Cell Proliferation Assay: The MTT (3-[4,5-dimethylthiazol-2-yl]-2,5-diphenyltetrazolium bromide) tetrazolium reduction assay was the first homogeneous cell viability assay developed for a 96-well format that was suitable for high throughput screening (HTS) and was broadly used to measure the in-vitro cytotoxic effects of drugs on cell lines or primary patient cells.

Reagents: PBS, MTT (5 mg mL^{-1} in PBS) (Hi-Media) – filtered and kept in dark, freshly prepared dimethyl sulfoxide (DMSO) (Hi-Media), 96-well plate (flat bottom).

Procedure: The MTT assay was used to determine the cytotoxicity of GO composites in A549 cell line. 1.48×10^3 cells per well/100 µL was seeding density. Cells were plated into 96-well tissue culture plates and allowed to attach overnight at 37 °C. Afterwards, cells were treated with increasing concentrations of a GO and GO/MO composites. The range used to check IC50 (inhibitory concentration) value was 400–6.25 µg mL^{-1} for GO, GO/Cu_2O, and GO/Fe_3O_4 and 500–7.8 µg mL^{-1} for GO/TiO_2. After 24 h, MTT (5 mg mL^{-1}, Hi-Media) was added to each well and plate was incubated at 37 °C for 4 h. Then, 100 µL of DMSO was added to each well and mixed thoroughly to dissolve the formazan crystals. Optical density (OD) was measured at 570 nm using an ELISA reader (Multiskan spectrum microplate reader, Thermo scientific).

Characterization: Philips X'Pert MPD system using Cu Kα radiation with 1.54 Å for scattering angle (2θ) range 1°–80° was used for XRD measurement. SEM images were obtained using LEO microscope after gold sputter coating. JEOL, JEM 2100 microscope with an accelerating voltage up to 200 keV was used for the TEM measurements. FTIR spectra of GO and GO/MO composites was done using KBr pellet method with a spectrum GX series 49387 spectrometer in the frequency range 4000–400 cm^{-1}. Raman measurements were carried out using AIRIX STR-500 Raman spectrometer with 532 nm laser radiation. TGA measurements were carried out under nitrogen atmosphere on Mettler Toledo TGA/SDTA851e with stare software, with a heating rate of 10 °C min^{-1}.

Conflict of Interest

The authors declare no conflicts of interest.

Data Availability Statement

Data available on request from the authors.

Keywords

anticancer activity, graphene oxide, metal oxide

Received: April 5, 2023
Revised: September 23, 2023

[1] L. Zou, L. Wang, Y. Wu, C. Ma, S. Yu, X. Liu, *J. Data Inf. Sci.* **2018**, *3*, 82.
[2] D. Chen, H. Feng, J. Li, *Chem. Rev.* **2012**, *112*, 6027.
[3] K. Chen, Q. Wang, Z. Niu, J. Chen, *J. Energy Chem.* **2018**, *27*, 12.
[4] X. Wang, G. Shi, *Energy Environ. Sci.* **2015**, *8*, 790.
[5] Y. Zhu, S. Murali, W. Cai, X. Li, J. W. Suk, J. R. Potts, R. S. Ruoff, *Adv. Mater.* **2010**, *22*, 3906.
[6] M. Lotya, Y. Hernandez, P. J. King, R. J. Smith, V. Nicolosi, L. S. Karlsson, F. M. Blighe, S. De, Z. Wang, I. T. McGovern, G. S. Duesberg, *J. Am. Chem. Soc.* **2009**, *131*, 3611.
[7] D. Li, M. B. Müller, S. Gilje, R. B. Kaner, G. G. Wallace, *Nat. Nanotechnol.* **2008**, *3*, 101.
[8] S. Mohamadi, M. Hamidi, in *Nanostructures for Drug Delivery*, Elsevier, **2017**, pp. 107–147.
[9] J. Liu, J. Dong, T. Zhang, Q. Peng, *J. Controlled Release* **2018**, *286*, 64.
[10] M. Nurunnabi, K. Parvez, M. Nafiujjaman, V. Revuri, H. A. Khan, X. Feng, Y. K. Lee, *RSC Adv.* **2015**, *5*, 42141.
[11] M. Zhang, N. Zhou, P. Yuan, Y. Su, M. Shao, C. Chi, *RSC Adv.* **2017**, *7*, 9284.
[12] L. Yi, Y. Zhang, X. Shi, X. Du, X. Wang, A. Yu, G. Zhai, *J. Drug Target.* **2019**, *27*, 125.
[13] M. Nurunnabi, Z. Khatun, G. R. Reeck, D. Y. Lee, Y. K. Lee, *ACS Appl. Mater. Interfaces* **2014**, *6*, 12413.
[14] J. Tang, Q. Chen, L. Xu, S. Zhang, L. Feng, L. Cheng, H. Xu, Z. Liu, R. Peng, *ACS Appl. Mater. Interfaces* **2013**, *5*, 3867.
[15] X. Zhang, W. Hu, J. Li, L. Tao, Y. Wei, *Toxicol. Res.* **2012**, *1*, 62.
[16] G. G. Montes-Duarte, G. Tostado-Blázquez, K. L. S. Castro, J. R. Araujo, C. A. Achete, J. L. Sánchez-Salas, J. Campos-Delgado, *RSC Adv.* **2021**, *11*, 6509.
[17] M. Behera, G. Giri, *Int. J. Ind. Chem.* **2016**, *7*, 157.
[18] X. Zhang, J. Song, J. Jiao, X. Mei, *Solid State Sci.* **2010**, *12*, 1215.
[19] T. Miyata, K. Watanabe, H. Tokunaga, T. Minami, *J. Semicond.* **2019**, *40*, 032701.
[20] Y. Lin, H. Wan, F. Chen, X. Liu, R. Ma, T. Sasaki, *Dalton Trans.* **2018**, *47*, 7694.
[21] C. Dong, M. Zhong, T. Huang, M. Ma, D. Wortmann, M. Brajdic, I. Kelbassa, *ACS Appl. Mater. Interfaces* **2011**, *3*, 4332.
[22] C. Hou, H. Quan, Y. Duan, Q. Zhang, H. Wang, Y. Li, *Nanoscale* **2013**, *5*, 1227.
[23] P. Anbu, S. C. B. Gopinath, K. Saravanakumar, S. Vijayakumar, S. Ramanathan, M.-H. Wang, *J. Environ. Chem. Eng.* **2021**, *9*, 105781.
[24] S. A. Khan, Z. Arshad, S. Shahid, I. Arshad, K. Rizwan, M. Sher, U. Fatima, *Composites, Part B* **2019**, *175*, 107120.
[25] S. M. Mousavi, S. A. Hashemi, A. Gholami, N. Omidifar, M. Zarei, S. Bahrani, K. Yousefi, W.-H. Chiang, A. Babapoor, *Bioinorg. Chem. Appl.* **2021**, *2021*.
[26] S. Lettieri, M. Pavone, A. Fioravanti, L. S. Amato, P. Maddalena, *Materials* **2021**, *14*, 1645.
[27] B. Salama, E. S. El-Sherbini, G. El-Sayed, M. El-Adl, K. Kanehira, A. Taniguchi, *Int. J. Mol. Sci.* **2020**, *21*, 605.
[28] F. Fujishima, in *A Revolution in Cleaning Technology*, **1999**, pp. 14.
[29] Z. Hu, Y. Huang, S. Sun, W. Guan, Y. Yao, P. Tang, C. Li, *Carbon* **2012**, *50*, 994.
[30] M. Nowostawska, S. A. Corr, S. J. Byrne, J. Conroy, Y. Volkov, Y. K. Gun'ko, *J. Nanobiotechnol.* **2011**, *9*, 13.
[31] G. Simonsen, M. Strand, G. Øye, *J. Pet. Sci. Eng.* **2018**, *165*, 488.
[32] I. M. El-Sherbiny, N. M. Elbaz, M. Sedki, A. Elgammal, M. H. Yacoub, *Nanomedicine* **2017**, *12*, 387.
[33] S. P. Schwaminger, S. A. Blank-Shim, I. Scheifele, V. Pipich, P. Fraga-García, S. Berensmeier, *Biotechnol. J.* **2019**, *14*, 1800055.
[34] L. Yi, Y. Huang, T. Wu, J. Wu, *Neural Regen. Res.* **2013**, *8*, 3036.
[35] T. M. Zimina, N. O. Sitkov, K. G. Gareev, V. Fedorov, D. Grouzdev, V. Koziaeva, H. Gao, S. E. Combs, M. Shevtsov, *Biosensors* **2022**, *12*, 789.
[36] S. Khizar, E. Elkalla, N. Zine, N. Jaffrezic-Renault, A. Errachid, A. Elaissari, *Expert Opin. Drug Deliv.* **2023**, *20*, 189.
[37] S. Liu, J. Fu, M. Wang, Y. Yan, Q. Xin, L. Cai, Q. Xu, *J. Colloid Interface Sci.* **2016**, *469*, 69.
[38] X. Fu, J. Liu, X. He, *Colloids Surf. A* **2014**, *453*, 101.
[39] D. Yu, X. Sun, J. Zou, Z. Wang, F. Wang, K. Tang, *J. Phys. Chem. B* **2006**, *110*, 21667.
[40] A. Taheri-Kafrani, H. Shirzadfar, A. A. Kajani, B. K. Kudhair, L. J. Mohammed, S. Mohammadi, F. Lotfi, *J. Biotechnol.* **2021**, *331*, 26.
[41] A. Alizadeh, G. Abdi, M. M. Khodaei, M. Ashokkumar, J. Amirian, *RSC Adv.* **2017**, *7*, 14876.
[42] L. Debbichi, M. C. Marco de Lucas, J. F. Pierson, P. Kruger, *J. Phys. Chem. C* **2012**, *116*, 10232.
[43] Y. X. Li, J. Zhu, Y. Chen, J. Zhang, J. Wang, B. Zhang, Y. He, W. J. Blau, *Nanotechnology* **2011**, *22*, 205704.
[44] P. Wang, Y. Zhai, D. Wang, S. Dong, *Nanoscale* **2011**, *3*, 1640.
[45] K. S. Novoselov, A. K. Geim, S. V. Morozov, D. Jiang, Y. Zhang, S. V. Dubonos, I. V. Grigorieva, A. A. Firsov, *Science* **2004**, *306*, 666.
[46] D. R. Dreyer, S. Park, C. W. Bielawski, R. S. Ruoff, *Chem. Soc. Rev.* **2010**, *39*, 228.
[47] M. Fiorillo, A. F. Verre, M. Iliut, M. Peiris-Pagés, B. Ozsvari, R. Gandara, A. R. Cappello, F. Sotgia, A. Vijayaraghavan, M. P. Lisanti, *Oncotarget* **2015**, *6*, 3553.
[48] C. Jin, F. Wang, Y. Tang, X. Zhang, J. Wang, Y. Yang, *Biol. Trace Elem. Res.* **2014**, *159*, 393.
[49] J. Wang, J. Fang, P. Fang, X. Li, S. Wu, W. Zhang, S. Li, *J. Biomater. Sci., Polym. Ed.* **2017**, *28*, 337.
[50] S. Mittal, V. Kumar, N. Dhiman, L. K. S. Chauhan, R. Pasricha, A. K. Pandey, *Sci. Rep.* **2016**, *6*, 39548.
[51] V. Chabot, D. Higgins, A. Yu, X. Xiao, Z. Chen, J. Zhang, *Energy Environ. Sci.* **2014**, *7*, 1564.
[52] W. S. Hummers Jr, R. E. Offeman, *J. Am. Chem. Soc.* **1958**, *80*, 1339.
[53] B. Zeng, X. Chen, X. Ning, C. Chen, W. Deng, Q. Huang, W. Zhong, *Appl. Surf. Sci.* **2013**, *276*, 482.